

## Supplementary Information: Direct Observation of a Uniaxial Stress-driven Lifshitz Transition in $\text{Sr}_2\text{RuO}_4$

Veronika Sunko<sup>1,2</sup>, Edgar Abarca Morales<sup>1,2</sup>, Igor Marković<sup>1,2</sup>, Mark E. Barber<sup>1</sup>, Dijana Milosavljević<sup>1</sup>, Federico Mazzola<sup>2</sup>, Dmitry A. Sokolov<sup>1</sup>, Naoki Kikugawa<sup>3</sup>, Cephise Cacho<sup>4</sup>, Pavel Dudin<sup>4</sup>, Helge Rosner<sup>1</sup>, Clifford W. Hicks<sup>1,\*</sup>, Philip D.C. King<sup>2,\*</sup> and Andrew P. Mackenzie<sup>1,2,\*</sup>

<sup>1</sup> Max Planck Institute for Chemical Physics of Solids, Nöthnitzer Strasse 40, 01187 Dresden, Germany

<sup>2</sup> SUPA, School of Physics and Astronomy, University of St. Andrews, St. Andrews KY16 9SS, United Kingdom

<sup>3</sup> National Institute for Materials Science, Tsukuba, Ibaraki 305-0003, Japan.

<sup>4</sup> Diamond Light Source, Harwell Campus, Didcot, OX11 0DE, United Kingdom.

\* to whom correspondence should be addressed: [Clifford.Hicks@cpfs.mpg.de](mailto:Clifford.Hicks@cpfs.mpg.de); [philip.king@st-andrews.ac.uk](mailto:philip.king@st-andrews.ac.uk); [Andy.Mackenzie@cpfs.mpg.de](mailto:Andy.Mackenzie@cpfs.mpg.de)

### 1) Spring-based rig

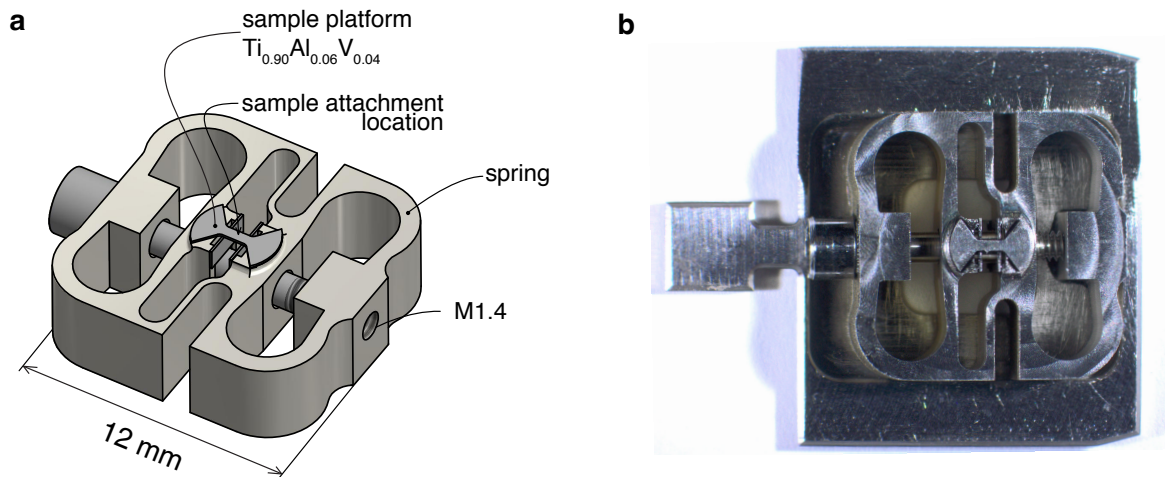


**Fig. S1: The spring-based rig.** (a) An illustration of the spring-based rig, actuated by *ex-situ* turning of the adjustment screw. The spring constant of the spring ( $0.8 \text{ N}/\mu\text{m}$ ) is designed to be 10 times smaller than that of the sample substrate. A displacement caused by turning the M1.4 screw by half a turn ( $0.15 \text{ mm}$ ) results in a sample platform strain of  $\sim 1\%$ , as confirmed by optical analysis of the strained platform. Both the spring and the substrate were made of Grade 5 titanium ( $\text{Ti}_{0.90}\text{Al}_{0.06}\text{V}_{0.04}$ ). (b) A photograph of the spring-based rig mounted on a standard flag-style sample plate.

## 2) Sample and platform characterisation

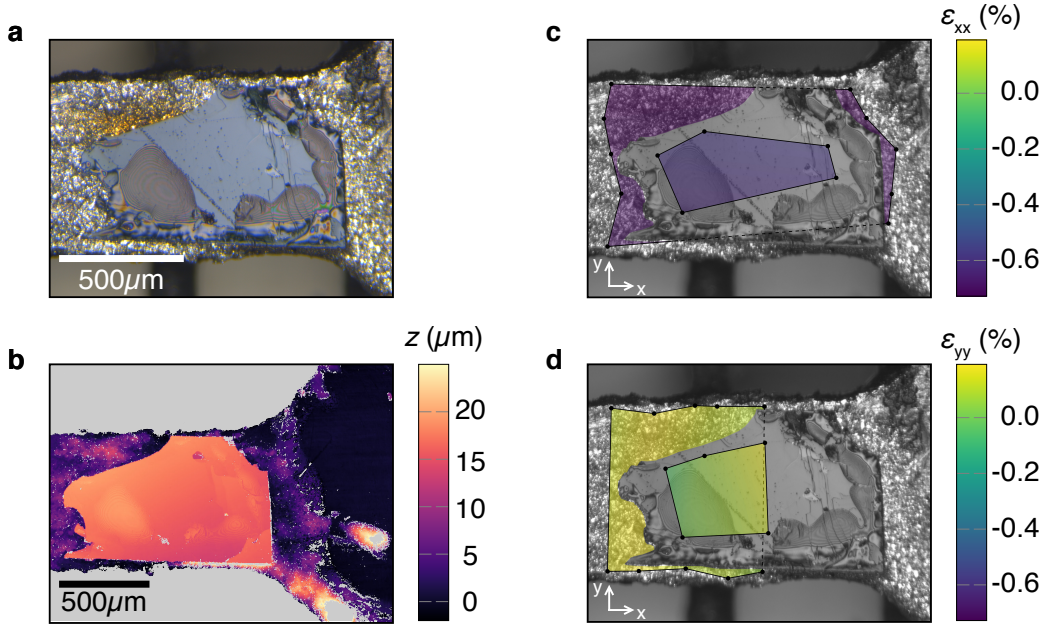


**Fig. S2: Platform and sample strain determination.** (a) An optical micrograph of the maximally-strained sample, the data from which are shown in Figs. 2–4, taken after the ARPES measurements. (b) The thickness of the sample and epoxy measured with an optical profilometer. (c)-(d) The strain achieved in the sample and platform was determined by tracking the relative displacement of features on their surfaces (indicated by the dots) as the device was cooled down in an optical cryostat. The average strain developed by cooling from room temperature to  $\sim 10$  K was found to be  $\epsilon_{xx} = -0.61 \pm 0.03\%$  and  $\epsilon_{yy} = +0.05 \pm 0.10\%$  in the sample, and  $\epsilon_{xx} = -0.71 \pm 0.02\%$  and  $\epsilon_{yy} = +0.12 \pm 0.07\%$  in the platform. These values correspond to anisotropic strains of  $\epsilon_{xx} - \epsilon_{yy} = -0.7 \pm 0.1\%$  in the sample, and  $-0.8 \pm 0.1\%$  in the platform, as quoted in the main text.

The best current estimate of the strain value at which the peak in  $T_c$  and associated anomalies in the electronic properties of  $\text{Sr}_2\text{RuO}_4$  are observed is obtained by measurements on free-beam samples using a calibrated force sensor<sup>1</sup>. They showed that the peak in low-temperature resistivity is reached for a uniaxial pressure of 0.7 GPa, a value that can be converted to an anisotropic strain of  $\epsilon_{xx} - \epsilon_{yy} = -0.55\%$  using the known room-temperature values for Young's modulus and Poisson's ratio (176 GPa and 0.39, respectively<sup>2</sup>). The  $T_c$  peaks at a strain  $\sim 10\%$  higher than the low-temperature resistivity<sup>3</sup>, i.e. at an anisotropic strain of  $\epsilon_{xx} - \epsilon_{yy} = -0.61\%$ .

### 3) Strain-dependent ARPES data

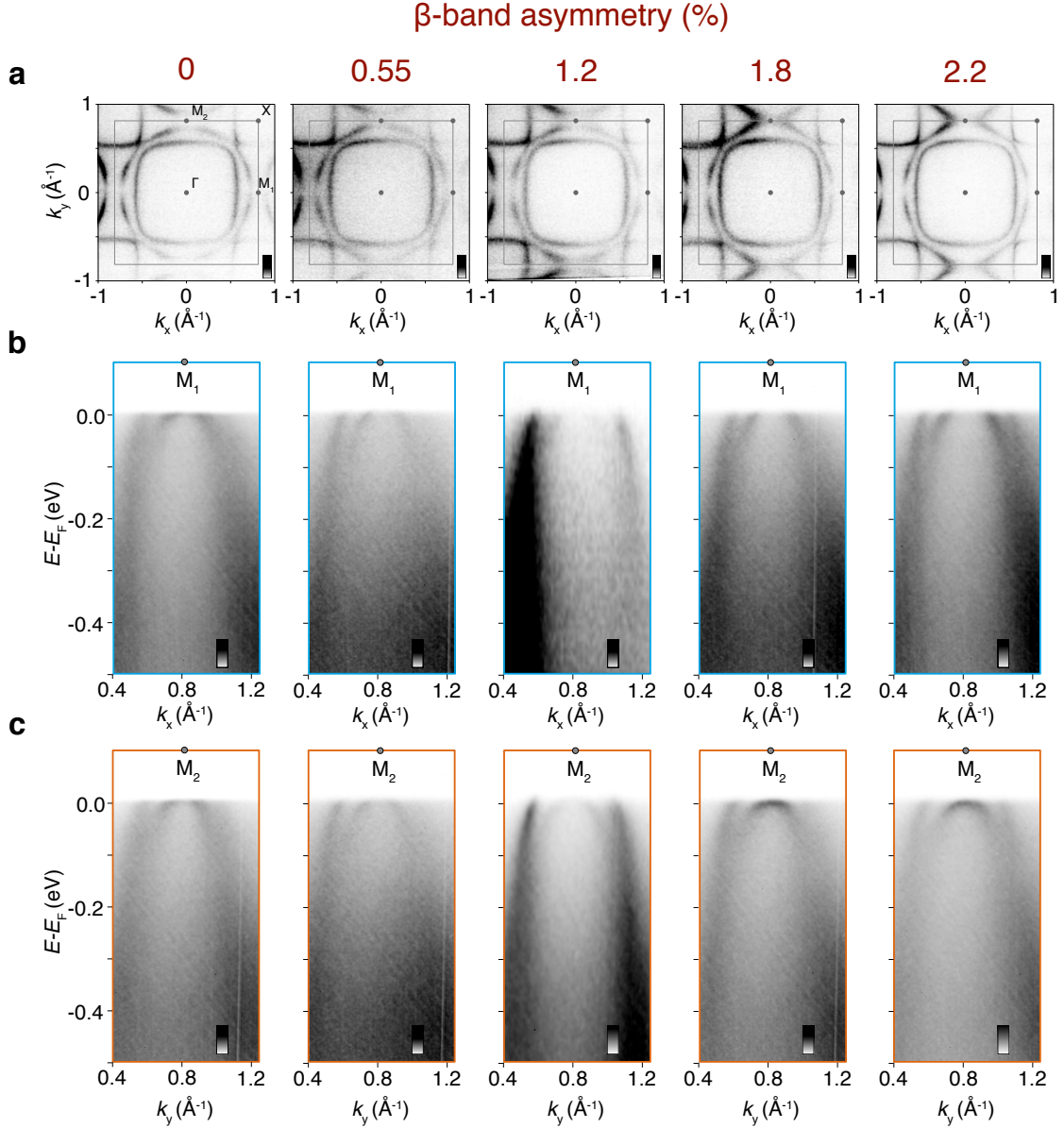


**Fig. S3: Strain-dependent ARPES measurements.** Measured (a) Fermi surfaces and (b,c) dispersions along the (b)  $\Gamma$ - $M_1$  and (c)  $\Gamma$ - $M_2$  direction from samples under different strain, as encoded by their varying  $\beta$ -band asymmetries. The measurements of the unstrained sample ( $\beta$ -band asymmetry of 0%) were taken on a standard sample plate, while the measurements at the  $\beta$ -band asymmetry of 1.2% were taken on a sample mounted on the spring-based cell (Fig. S1). All other samples were mounted on the differential thermal contraction sample stage (Fig. 1 of the main text). All the Fermi surface maps were measured using a photon energy of 68eV, as were the dispersions at the  $\beta$ -band asymmetry of 1.2%. All other dispersions were measured using a photon energy of 40eV. All measurements were taken using  $p$ -polarised light. The points in Fig. 5(a,c) of the main text were extracted from fitting of these measured dispersions and Fermi surfaces, respectively. Extracting Fermi momenta along the high symmetry directions from the Fermi surface maps would be less precise because of the matrix element suppression along those lines (see Fig. 2(b)).

#### 4) Insensitivity of calculated Fermi surface anisotropies on Poisson's ratio

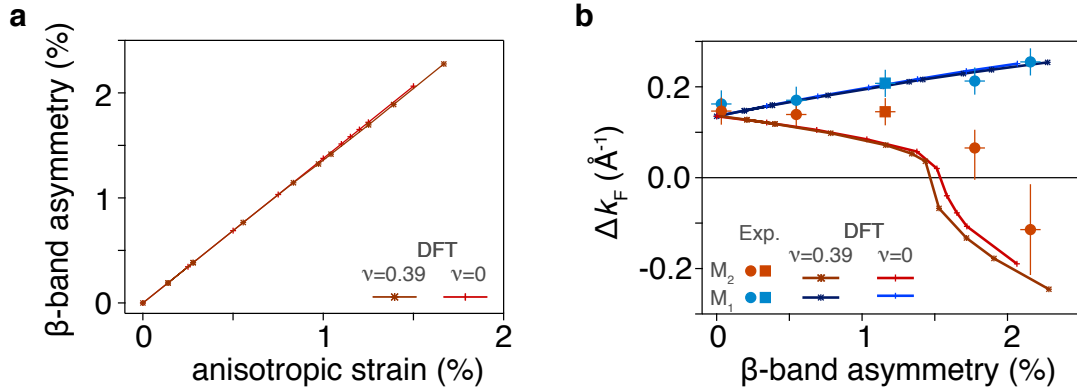


**Fig. S4: Insensitivity of calculated Fermi surface anisotropies on Poisson's ratio.**

(a) The  $\beta$ -band asymmetry as a function of the absolute value of the anisotropic strain,  $|\varepsilon_{xx}-\varepsilon_{yy}|$ , as calculated by DFT for  $\text{Sr}_2\text{RuO}_4$  with its experimental Poisson's ratio of  $\nu = 0.39$ , and assuming a pure uniaxial strain ( $\nu = 0$ ). The calculated  $\beta$ -band asymmetry is linear with anisotropic strain, with a slope independent of Poisson's ratio, confirming  $\beta$ -band asymmetry as a useful internal metric of anisotropic strain. (b) Parametrization of the  $\gamma$ -sheet anisotropy, as a function of uniaxial strain encoded via the  $\beta$ -sheet anisotropy (same as Figure 5a of the main text). DFT calculations are performed using the experimental Poisson's ratio of  $\nu = 0.39$ , as well as assuming a pure uniaxial strain ( $\nu = 0$ ). The good agreement between the two calculations shows that the discrepancy between DFT and experiment cannot be accounted for by the fact the sample on the platform expands according to the Poisson ratio of the platform, rather than the sample.

#### References

1. Barber, M. E., Steppke, A., Mackenzie, A. P. & Hicks, C. W. Piezoelectric-based uniaxial pressure cell with integrated force and displacement sensors. *Rev. Sci. Instrum.* 90, 023904 (2019).
2. Paglione, J. *et al.* Elastic tensor of  $\text{Sr}_2\text{RuO}_4$ . *Phys. Rev. B* 65, (2002).
3. Barber, M. E., Gibbs, A. S., Maeno, Y., Mackenzie, A. P. & Hicks, C. W. Resistivity in the Vicinity of a van Hove Singularity:  $\text{Sr}_2\text{RuO}_4$  under Uniaxial Pressure. *Phys. Rev. Lett.* 120, 076602 (2018).